Journal of the Serbian Chemical Society
JSCS-info@shd.org.rs • www.shd.org.rs/JSCS

ACCEPTED MANUSCRIPT

Journal of the Serbian Chemical Society
JSCS-info@shd.org.rs • www.shd.org.rs/JSCS
J. Serb. Chem. Soc. **00(0)** 1-15 (2026)
JSCS–13582
Original scientific paper
Published DD MM, 2026

Design of novel quinazoline-chalcone hybrids as potent epidermal growth factor receptor inhibitors

YINGNUO WANG[1], JURANG LI[1], CHUNMENG LI[1], YANG LIU[1], ZHIQIANG CAI[1]*, AND SHUAI LI[2†]

[1]Liaoning Province Professional and Technical Innovation Center for Fine Chemical Engineering of Aromatics Downstream, School of Petrochemical Engineering, Shenyang University of Technology, Liaoning, Liaoyang 111003, P. R. China, and [2]Shandong Engineering Research Center of Pharmaceutical Green Intelligent Technology, Shandong Academy of Pharmaceutical Sciences, Shandong, Jinan 250101, P. R. China.

(Received 13 October 2025; revised 4 June 2026; accepted 13 August 2026)

Abstract: This study successfully designed and synthesized a novel series of quinazoline-chalcone hybrids. The key innovation lies in the molecular hybridization of the pharmacophoric quinazoline scaffold with a chalcone moiety, creating new chemical entities to exploit potential synergistic antitumor effects. A concise multi-step synthetic route was efficiently implemented. Preliminary evaluation demonstrated that a majority of these hybrids exhibited potent antiproliferative activity against non-small cell lung cancer (NSCLC) cell lines (A549 and H1975) *in vitro*. Molecular docking studies suggested against epidermal growth factor receptor (EGFR) inhibition as a potential mechanism, with the compounds forming stable interactions with the kinase domain. Furthermore, in silico absorption, distribution, metabolism, and excretion (ADME) and toxicity predictions by SwissADME and ProTox 3.0, respectively, indicated promising drug-like properties and safety profiles. However, the cytotoxicity was assessed only on cancer cell lines, and the selectivity against normal cells remains to be determined. Despite this limitation, the compelling initial results position these novel hybrids as promising leads for future optimization and development.

Keywords: synthesis; EGFR inhibition; molecular docking; antitumor activity; ADME prediction; structure-activity relationship.

INTRODUCTION

Targeted therapies achieve precision treatment by specifically inhibiting key signaling pathways in cancer cells.[1-5] The 4-aminoquinazoline scaffold serves as a

* Corresponding authors. E-mails: kahongzqc@163.com; †627174596@qq.com
https://doi.org/10.2298/JSC251013048W

privileged pharmacophore that forms the structura- l basis of multiple clinically approved EGFR tyrosine kinase inhibitors (EGFR-TKIs),[6-9] such as **zorifertinib**.[10] Its high structural versatility enables rational optimization of inhibitory activity against specific mutations. Meanwhile, natural chalcone derivatives exhibit broad-spectrum antitumor effects through their ⟨,®-unsaturated ketone moiety,[11-14] which modulates diverse oncogenic processes via multiple mechanisms. The present study innovatively integrates the quinazoline core with chalcone structures using flexible linkers.[15-17] It preserves the critical hydrogen-bonding network between the quinazoline scaffold and EGFR's adenosine triphosphate (ATP)-binding pocket while leveraging chalcone's covalent binding capability to enhance target engagement.[18] The systematic molecular optimization through bioisosteric replacement and pharmacophore refinement generated novel small-molecule inhibitors with improved selectivity and pharmacokinetic profiles.[19-21]

The molecular design strategy is illustrated in **Fig. 1**: The third-generation EGFR inhibitor **zorifertinib** demonstrates a characteristic binding mode wherein the N3 nitrogen atom of the quinazoline core establishes a hydrogen-bonding interaction with the catalytic residue ASP-855 of the target protein. The molecular scaffold occupies the ATP-binding pocket delineated by ARG748, GLY857, ASP855, LYS875, and GLY874 residues, with 6- and 7- position substituents projecting into the solvent-accessible region. This binding conformation exemplifies the conserved structural motif of quinazoline-derived EGFR inhibitors. Accordingly, a rational design strategy was implemented by introducing flexible linkers containing chalcone structures at the 6- position. The ⟨,®-unsaturated ketone moiety serves as a Michael acceptor to form selective covalent bonds with target protein residues while the aromatic system enhances binding affinity through hydrophobic interactions.[22-26] Additionally, the methoxy group at this position is retained to synergistically improve antitumor activity and mutation selectivity.[27] Based on the above structure-activity relationship analysis, the present study adopted highly selective pharmacophores as the molecular design framework and innovatively constructed a hybrid quinazoline-chalcone molecular system. By integrating the protein-binding patterns and structure-activity relationship data of **zorifertinib**, this study precisely preserved the quinazoline core structure of EGFR inhibitors using the bioisosterism principle,[28,29] while systematically optimizing the pharmacokinetic properties of candidate compounds through pharmacophore refinement and isosteric replacement strategies. Through rational design, a series of novel small-molecule EGFR inhibitors featuring combined quinazoline and chalcone structural motifs were successfully developed.

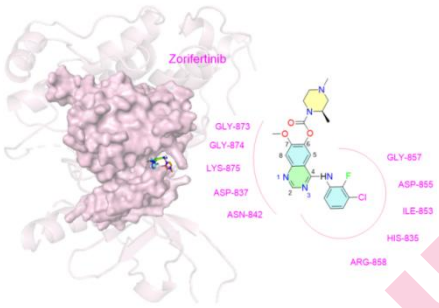

Fig. 1. Zorifertinib Molecular Docking Interaction Diagram.

Based on the aforementioned research background, the present study synthesized and characterized a series of novel quinazoline-chalcone hybrids using IR, ^{1}H NMR, ^{13}C NMR. and mass spectrometry. Their antitumor activities were evaluated against A549 and H1975 cell lines. In addition, in silico ADME prediction, toxicity prediction, and molecular docking with the EGFR kinase domain (PDB: 7OXB) were performed to assess drug-like properties and explore the binding mode of representative compound **9h**, providing mechanistic insights into its action.

EXPERIMENTAL

Chemistry

General. All reagents and solvents were commercially available and used as received unless otherwise specified. Reaction progress was monitored by thin-layer chromatography (TLC) on pre-coated silica gel GF254 plates (Qingdao Haiyang Chemical Co., Ltd.).

Instrumentation and Characterization. Melting points were determined on an X-4 micro-melting point apparatus and are uncorrected. ^{1}H NMR and ^{13}C NMR spectra were recorded on a Bruker ARX-400 spectrometer (400 MHz for ^{1}H NMR, 101 MHz for ^{13}C NMR) in the indicated deuterated solvents ($CDCl_3$ or DMSO-d_6) using tetramethylsilane (TMS) as an internal standard; chemical shifts are reported in ppm (^{TM}) and coupling constants (J) are given in Hertz (Hz). FT-IR spectra were acquired on a Bruker TENSOR II spectrometer using KBr pellets, and wavenumbers are reported in cm^{-1}. Low-resolution electrospray ionization (ESI) mass spectra were recorded on a Finnigan Trace MS spectrometer. Samples were dissolved in a mixed solvent of methanol and acetonitrile and introduced via direct infusion in positive ion mode. All observed m/z values corresponded to the expected $[M]^+$ or $[M+H]^+$ ions of the target compounds.

*General procedure for the synthesis of intermediates **2**.*

Specific synthesis process: At room temperature, the mixed solution of 7-methoxy-4-oxo-3,4-dihydroquinazolin-6-yl acetate **1** (1.20 g, 5.12 mmol), toluene (15 mL), a.nd triethylamine (0.88 g, 8.71 mmol) were heated to 80℃. Then, phosphorus oxychlo ride (1.96 g, 12.81 mmol) was added to the mixture. After completion, the reaction proceeds directly to the next step.

General procedure for the synthesis of intermediates ***3a-3h***.[30]

Specific synthesis process: Substituted aniline (0.48 g, 4.35 mmol) was added to intermediate **2**, and the mixture was stirred for 5 h. After completion, the solvent was concentrated under vacuum and mixed with isopropanol (15 mL) for 12 h. The product was filtered to afford intermediate **3**.

General procedure for the synthesis of intermediates ***4a-4h***.[30]

Specific synthesis process: Intermediate **3** (1.00 g, 3.06 mmol), methanol (15 mL), and ammonia solution (1 mL) were stirred at room temperature. After completion. The solvent was concentrated under vacuum, followed by addition of water (8 mL). It was filtered to afford intermediate **4**.

General procedure for the synthesis of intermediates ***7a-7c***.

Specific synthesis process: Refer to references,[31] Taking (2*E*)-1-(4-aminophenyl)-3-(3-methylphenyl)prop-2-en-1-one (**6a**) as an example: 4-aminoacetop-henone (1.00 g, 3.70 mmol), 3-methylbenzaldehyde (0.88 g, 3.70 mmol), and ethanol (15 mL) were added sequentially, the reaction vessel was transferred to a cooling bath maintained at 5°C. Add a 20% aqueous sodium hydroxide (0.29 g, 7.40 mmol) solution dropwise over 0.25 h. After completion, the solvent was concentrated under vacuumto afford intermediates **7a**. The reaction proceeds directly to the next step.

General procedure for the synthesis of intermediates ***8a-8c***.[32]

Specific synthesis process: Taking *N*-{4-[(2*E*)-3-(3-methylphenyl)-1-oxop -rop-2-en-1-yl]phenyl}-2-chloroacetamide (7a) as an example: Intermediate **7a** (1.00 g, 4.21 mmol), dichloromethane (15 mL), chloroacetyl chloride (1.43 g, 12.64 mmol), and triethylamine (0.51 g, 5.06 mmol) were stirred at 0°C under nitrogen in a cooling bath. After completion, the mixture was warmed to 25°C and stirred for 6 h. The solvent was concentrated under vacuum to afford intermediates **8a**.

General procedure for the synthesis of compounds ***9a-9k***.

Specific synthesis process: Taking N-{4-[(2*E*)-3-(3-methylphenyl)-1-oxoprop- 2-en-1-yl]phenyl}-2-{[7-methoxy-4-(phenylamino)quinazolin-6-yl]oxy}acetamide(**9a**) as an example: A mixture of intermediate **4a** (0.50 g, 1.69 mmol), intermediate **8a** (0.58 g, 1.86 mmol), potassium carbonate (0.47 g, 3.39 mmol), and *N,N*-Dimethylformamide (10 mL) was heated to 80°C. After completion, water (20 mL) was added to the mixture, followed by filtration. The filter cake was collected and dried at 50°C, then purified by column chromatography to afford the final product.

Pharmacological experiments of target compounds.

Cell culture. The human NSCLC cell lines A549 and H1975 were obtained from the Shanghai Institute of Life Sciences, Chinese Academy of Sciences. Cells were cultured in RPMI 1640 medium (Invitrogen) supplemented with 10% fetal bovine serum (FBS, Invitrogen) in a humidified incubator at 37°C under an atmosphere of 5% CO_2. The cells were passaged using 0.25% trypsin (Amresco) upon reaching approximately 90% confluence.

Cell viability assay (CCK-8).The antiproliferative activity of the synthesized compounds was assessed using the CCK-8 (Wuhan Heyan Biotechnology). Briefly, cells in the logarithmic growth phase were digested, centrifuged, and resuspended in complete medium. Cell density was adjusted to 3×10^4 cells/mL using a hemocytometer. Subsequently, 100 μL of the cell suspension was seeded into each well of a 96-well plate (NEST Biotechnology) and incubated

for 24 h to allow attachment. After incubation, the medium was removed and replaced with 100 ⌈L of fresh medium containing various concentrations of the test compounds or the positive control (**Zorifertinib**). Cells treated with medium containing an equivalent volume of DMSO served as the negative control. The plates were then incubated for 72 h. Following the treatment period, 10 ⌈L of CCK-8 reagent was added to each well, and the plates were incubated for an additional 2 h. The absorbance at 450 nm was measured using a multifunctional microplate reader (Shanghan Hanfei Medical Instrument Co., Ltd.). The inhibition rate (*IR*%) was calculated using the following formula:

$$IR\% = \frac{OD_{\text{sample}} - OD_{\text{negative control}}}{OD_{\text{STSP}} - OD_{\text{negative control}}} \times 100\% \quad (1)$$

The half-maximal inhibitory concentration (IC_{50}) values were determined from concentration–response curves using GraphPad Prism software via nonlinear regression analysis (Bliss method). All experiments were performed in triplicate wells and repeated independently at least three times.

Molecular docking protocol.

Molecular docking of target derivatives with EGFR (PDB ID: 7OXB) was performed using AutoDock Vina. Small molecule ligands were prepared in ChemDraw/Chem3D and converted to PDBQT format alongside the pretreated protein. Following binding pocket configuration, 20 docking runs were conducted. Results were selected based on binding energy and conformation, with PyMOL used for interaction visualization.

The selection of the EGFR kinase domain (PDB ID: 7OXB) for molecular docking studies is based on its established relevance in elucidating the structural basis of quinazoline-based inhibitor binding. Although the anticancer activity was evaluated in whole-cell systems, docking simulations against the isolated kinase domain provide mechanistic insights into potential direct interactions with the EGFR target. The 7OXB structure represents a well-characterized model of the ATP-binding pocket and has been widely employed in structural studies of EGFR inhibitors. This approach allows for the prediction of key intermolecular interactions, such as hydrogen bonding and hydrophobic contacts, between the synthesized hybrids and critical residues (e.g., ASP-855, LYS-875), thereby supporting the interpretation of the observed structure–activity relationships and guiding future design strategies.

ADME prediction introduction.

ADME prediction is vital in drug development, using computational models to evaluate a compound's absorption, distribution, metabolism and excretion. Researchers simply input the molecular structure into a prediction platform and run the analysis. The system quickly generates key parameters like partition coefficients and permeability in standardized reports, enabling efficient lead compound optimization. This computer-aided approach significantly accelerates early-stage drug screening.

Toxicity prediction introduction.

Toxicity prediction is essential in drug development, using computational models to evaluate the safety profile of a compound. Researchers simply input the molecular structure into a prediction platform and run the analysis. The system quickly generates key parameters such as LD_{50} values and toxicity classes in standardized reports, enabling efficient identification of compounds with favorable safety margins. This computer-aided approach significantly reduces the risk of late-stage drug failure.

RESULTS AND DISCUSSION

Based on the synthesis methods of the references,[31-35] we systematically optimized the synthetic route for target compounds **9a-9k**, as illustrated in **Scheme 1.** Using 3,4-dihydro-7-methoxy-4-oxoquinazolin-6-yl acetate **1** as the starting material in toluene with triethylamine as the acid scavenger, we investigated the effect of reaction temperature on the chlorination with phosphorus oxychloride. As demonstrated in **Table SI**, optimal yields of 85-95% were achieved at 70°C for 2 h, whereas higher temperatures or prolonged reaction times led to increased byproduct formation. As shown in **Table SII**, intermediate **2** reacted with substituted anilines for 5 h to give intermediate **3** in high yield exceeding 90%, with both insufficient and excessive reaction times negatively impacting the yield. Subsequent alkaline hydrolysis of **3** with aqueous ammonia yielded intermediate **4**. In the synthesis of intermediates **7a-7c**, the influence of various basic conditions was systematically investigated. Using 4-aminoacetophenone and substituted benzaldehydes as starting materials, the reactions were conducted for 4 h under different basic conditions. As evidenced in **Table SIII**, the results demonstrated that sodium hydroxide afforded the highest product yield, while sodium carbonate showed reduced efficiency due to its weaker alkalinity and poor solubility. When triethylamine was employed as the base, the reaction yield was only approximately 50%. The results demonstrate that strong inorganic bases are more effective than weaker or organic bases in promoting the condensation. For intermediates **8a-8c**, optimization showed that a molar ratio of **7a-7c** to chloroacetyl chloride of 1.0:2.5 (**Table SIV**) and addition at 0°C (**Table SV**) afforded the best yield, avoiding incomplete conversion or bis-acylation. For the final etherification of **9a-9d**, 80°C proved optimal (**Table SVI**), balancing conversion and byproduct formation. Screening of bases (**Table SVII**) indicated that potassium carbonate, owing to its moderate basicity, effectively promoted alkoxide formation without triggering elimination side reactions, unlike sodium hydroxide which reduced yield through competitive elimination.

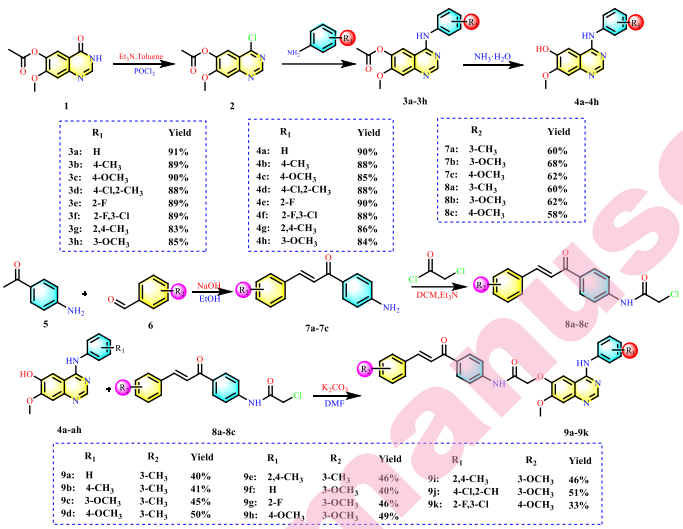

	R_1	Yield
3a:	H	91%
3b:	4-CH_3	89%
3c:	4-OCH_3	90%
3d:	4-Cl,2-CH_3	88%
3e:	2-F	89%
3f:	2-F,3-Cl	89%
3g:	2,4-CH_3	83%
3h:	3-OCH_3	85%

	R_1	Yield
4a:	H	90%
4b:	4-CH_3	88%
4c:	4-OCH_3	85%
4d:	4-Cl,2-CH_3	88%
4e:	2-F	90%
4f:	2-F,3-Cl	88%
4g:	2,4-CH_3	86%
4h:	3-OCH_3	84%

	R_2	Yield
7a:	3-CH_3	60%
7b:	3-OCH_3	68%
7c:	4-OCH_3	62%
8a:	3-CH_3	60%
8b:	3-OCH_3	62%
8c:	4-OCH_3	58%

	R_1	R_2	Yield		R_1	R_2	Yield		R_1	R_2	Yield
9a:	H	3-CH_3	40%	9e:	2,4-CH_3	3-CH_3	46%	9i:	2,4-CH_3	3-OCH_3	46%
9b:	4-CH_3	3-CH_3	41%	9f:	H	3-OCH_3	40%	9j:	4-Cl,2-CH	3-OCH_3	51%
9c:	3-OCH_3	3-CH_3	45%	9g:	2-F	3-OCH_3	46%	9k:	2-F,3-Cl	4-OCH_3	33%
9d:	4-OCH_3	3-CH_3	50%	9h:	4-OCH_3	3-OCH_3	49%				

Scheme 1. The synthesis route of target derivatives.

Through systematic optimization as described, we have established an efficient six-step synthetic route starting from 3,4-dihydro-7-methoxy-4-oxoquinazolin-6-yl acetate **1**, involving sequential chlorination, amination, hydrolysis, condensation, acylation, and etherification reactions. Each reaction condition was thoroughly investigated and optimized, with all key steps achieving satisfactory yields to provide sufficient compound samples for subsequent structure-activity relationship studies. This synthetic route demonstrates several advantageous characteristics including readily available starting materials, mild reaction conditions, and straightforward operational procedures.

Antitumor activity

The antitumor activity of the target compounds was evaluated using the CCK-8 assay *in vitro*. **Zorifertinib** was employed as the positive control drug. The inhibitory effects on A549 and H1975 cell lines are summarized in **Table I**.

The data in **Table I** demonstrate that the activity of target compounds is closely related to the type and position of R_1 and R_2 substituents in their structures. When R_2 was meta-methyl substituted, compounds **9d** and **9e** exhibited inhibitory rates of 49.82% and 54.27% against A549 cells, respectively, approaching the efficacy of the positive control **Zorifertinib** (62.14%). Notably, these compounds demonstrated more pronounced inhibitory effects against H1975 cells, with rates reaching 54.97% and 62.22% (compared to **Zorifertinib**'s 49.60% in this cell line). These results indicate that meta-methyl substitution can significantly enhance the inhibitory activity of compounds against H1975 cells. This enhancement effect may originate from the steric hindrance effect of meta-methyl optimizing the binding conformation between molecules and target proteins, while its

hydrophobicity strengthens interactions with active sites. Additionally, meta-substitution may reduce molecular conformational freedom, maintaining pharmacophores in a more favorable orientation, thereby improving inhibitory efficiency.

Table I. The inhibition rate of target compounds on tumor cells.

Compound	R_1	R_2	Inhibition rate %[a]	
			A549	H1975
9a	H	3-CH_3	-4.16	36.77
9b	4-CH_3	3-CH_3	0.12	36.17
9c	3-OCH_3	3-CH_3	23.80	20.06
9d	4-OCH_3	3-CH_3	54.27	62.22
9e	2,4-CH_3	3-CH_3	49.82	54.97
9f	H	3-OCH_3	36.55	58.99
9g	2-F	3-OCH_3	43.99	62.63
9h	4-OCH_3	3-OCH_3	47.80	58.17
9i	2,4-CH_3	3-OCH_3	14.96	35.25
9j	4-Cl,2-CH_3	3-OCH_3	41.63	34.45
9k	2-F,3-Cl	4-OCH_3	47.56	61.92
Zorifertinib	-	-	62.14	49.60

[a] Compounds concentration: 50 μM.

Further investigation of the meta-methoxy substituted compounds at the R_2 position revealed that **9j** (R_1 = 4-chloro-2-methyl), **9g** (R_1 = 2-fluoro), and **9h** (R_1 = 4-methoxy) exhibited inhibition rates of 41.63%, 43.99%, and 47.80% against A549 cells, respectively, all slightly lower than that of the positive control **Zorifertinib** (62.14%). In contrast, against H1975 cells, both **9g** (62.63%) and **9h** (58.17%) demonstrated significantly enhanced inhibitory activity compared to **Zorifertinib** (49.60%), whereas **9j** (34.45%) showed reduced potency. These results clearly indicate that with meta-methoxy substitution, the choice of R_1 substituent significantly impacts biological activity, with the 2-fluoro-substituted compound **9g** demonstrating particularly enhanced inhibition against H1975 cells, achieving an inhibition rate of 62.63%. The observed activity differences likely stem from the strong electronegativity of the 2-fluoro group facilitating improved hydrogen bonding interactions with the target protein, whereas the steric hindrance introduced by the 4-chloro, 2-methyl disubstitution in **9j** may impair optimal molecular binding to the target site.

Structure-activity relationship analysis demonstrated that the position of R_2 substituents critically influences biological activity. In H1975 cells, meta-substituted compounds **9e** (R_2 = 3-methyl) and **9g** (R_2 = 3-methoxy) demonstrated significantly superior inhibitory activities of 54.97% and 62.63%. This marked enhancement suggests that meta-substitution facilitates stronger molecular binding to the target protein. This advantage likely arises from the meta-substituents'

optimal accommodation within the three-dimensional architecture of the target's active site, improving spatial complementarity and hydrophobic interactions to enhance binding affinity. Furthermore, the structural characteristics of R_1 substituents exert a decisive influence on the antitumor activity of these compounds. Notably, compounds **9d** (R_1 = 4-methoxy) and **9e** (R_1 = 2,4-dimethyl) exhibited the most prominent inhibitory activities. Specifically, **9d** demonstrated inhibition rates of 54.27% and 62.22% against A549 and H1975 cell lines, respectively, while **9e** showed corresponding inhibition rates of 49.82% and 54.97%. Remarkably, compound **9g** (R_1 = 2-fluoro) displayed the strongest inhibitory activity against H1975 cells with an inhibition rate of 62.63%, although it exhibited relatively weaker activity against A549 cells (43.99% inhibition), indicating excellent cellular selectivity. Comprehensive analysis reveals that introducing medium-sized electron-donating groups (e.g., methoxy and methyl) at the R_1 position substantially enhances antitumor efficacy, with the 4-methoxy-substituted compounds **9d** and **9h** emerging as particularly promising drug candidates due to their optimal overall performance profile, rendering them promising candidates for further development.

According to the IC_{50} determination results shown in **Table II**, these compounds exhibited superior inhibitory activity against both A549 (IC_{50}: 7.479 μM) and H1975 (IC_{50}: 6.652 μM) cell lines compared to **Zorifertinib** (A549: 31.080 μM; H1975: 64.170 μM). Notably, compound **9e** demonstrated the lowest IC_{50} values (A549: 7.479 μM; H1975: 6.652 μM), indicating the most potent inhibitory effect. Furthermore, both **9d** (A549: 8.463 μM; H1975: 7.885 μM) and **9h** (A549: 7.944 μM; H1975: 8.739 μM) displayed IC_{50} values below 10 μM, further confirming their excellent antitumor potential. In conclusion, compounds **9e**, **9d**, and **9h** warrant further in-depth investigation due to their remarkable inhibitory activity and structural advantages.

Table II. IC_{50} value of **preferred** compounds.

Compound	IC_{50} (μM)	
	A549	H1975
9d	8.463	7.885
9e	7.479	6.652
9g	20.960	23.500
9h	7.944	8.739
9k	8.113	18.080
Zorifertinib	31.08	54.71

Preliminary structure-activity relationship analysis revealed several key patterns: First, the position of the R_2 substituent on the chalcone moiety had a decisive influence on activity with meta-substitution significantly outperforming para-substitution, likely due to its greater potential to form stable interactions with

the target protein. Second, methoxy-substituted compounds generally exhibited stronger activity than their methyl-substituted counterparts, suggesting the importance of hydrogen bonding in target recognition. Additionally, the number of R_1 substituents on the quinazoline moiety also affected activity with mono-substituted derivatives typically outperforming di-substituted analogs, possibly due to steric hindrance effects. These findings provide important guidance for the rational design of future antitumor drugs. In particular, the lead compound **9h** shows promising development potential and warrants further investigation into its pharmacological mechanisms and preclinical evaluation.

Molecular docking

Molecular docking of the positive control drug **zorifertinib** and selected target derivatives with EGFR kinase (PDB ID: 7OXB) was performed using AutoDock Vina. The binding modes between ligand molecules and receptor proteins were analyzed to further explore their interactions. The selected target derivative **9h** and the positive control drug **zorifertinib** were individually docked with the target protein EGFR.

The molecular docking analysis (**Fig. 2**, PDB: 7OXB) reveals that compound **9h** binds to EGFR primarily through an extensive hydrogen-bonding network. The quinazoline core forms critical hydrogen bonds with residues in the catalytic pocket (GLU-1015, GLN-820), while the side-chain substituents engage additional residues (GLN-812, ASN-816, TYR-813), collectively contributing to a stable and potent inhibition.

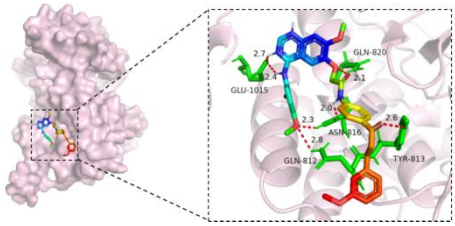

Fig. 2. Molecular docking models of compound **9h** with EGFR (PDB ID code: 7OXB).

Molecular docking of **zorifertinib** with EGFR (PDB: 7OXB, **Fig. 3**) reveals that its quinazoline core forms three key hydrogen bonds with the kinase domain: the 3-position nitrogen with ASP-855 (1.9 Å), the 4-position amino nitrogen with ASP-837 (2.3 Å), and the 6-position oxygen with LYS-875 (2.3 Å). These interactions, particularly the short, strong bond with ASP-855, are critical for anchoring the inhibitor tightly within the ATP-binding pocket. This binding network enhances stability and specificity, effectively competing with ATP to inhibit EGFR signaling and providing a structural basis for its potent antitumor activity.

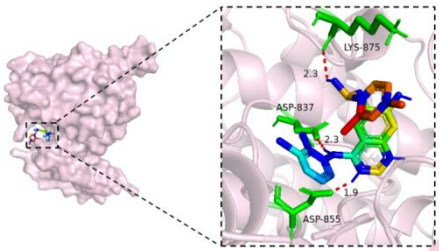

Fig. 3. Molecular docking models of **Zorifertinib** with EGFR (PDB ID code: 7OXB).

While both compound **9h** and **zorifertinib** share a conserved quinazoline core that targets the ATP-binding pocket of EGFR (PDB: 7OXB), their distinct side chains dictate divergent binding modes and inhibitory profiles. Compound **9h**, with its flexible C-6 substituent, engages the solvent-front region (GLN-812, TYR-813), potentially conferring adaptive binding to various mutants like L858R/T790M. In contrast, **zorifertinib**'s rigid structure deeply penetrates the back pocket, forming a strong salt bridge with ASP-855 in the DFG motif and a □-cation interaction with LYS-875, which may enhance its potency against wild-type EGFR. This analysis suggests that **9h**'s flexibility could be key for a broader mutant spectrum, whereas **zorifertinib**'s pre-organization favors strong wild-type inhibition.

Physicochemical properties and ADME prediction

As summarized in **Table III**, all synthesized compounds (**9a-9k**) exhibit molecular weights exceeding 500 Da, constituting a single Lipinski violation, while other key parameters such as TPSA (102.44-111.67 $Å^2$) and bioavailability scores (0.55) remain within favorable ranges. Despite the predicted low gastrointestinal absorption, the overall physicochemical profiles are typical of beyond-Rule-of-5 kinase inhibitors, and the potent in vitro antiproliferative activity against NSCLC cells demonstrates that these compounds can effectively reach their intracellular targets. The consistent drug-like parameters across the series, combined with their strong biological activity, highlight the potential of the quinazoline-chalcone hybrids as promising lead compounds for further optimization and development as novel anticancer agents.

Table III. Physicochemical properties and ADME properties of target compounds.

Comp.	MW (g/mol)	RB	HAcc <10	HDon	TPSA, Å≤140					[c]BS
9a	544.60	11	6	2	102.44	5.52	-7.02	Low	1*	0.55
9b	558.63	11	6	2	102.44	5.87	-7.33	Low	1*	0.55
9c	574.63	12	7	2	111.67	5.45	-7.11	Low	1*	0.55
9d	574.63	12	7	2	111.67	5.45	-7.11	Low	1*	0.55
9e	572.65	11	6	2	102.44	6.21	-7.63	Low	1*	0.55
9f	560.60	12	7	2	111.67	5.03	-6.80	Low	1*	0.55
9g	578.59	12	8	2	111.67	5.40	-6.96	Low	1*	0.55
9h	590.63	11	6	2	102.44	6.21	-7.11	Low	1*	0.55
9i	588.65	12	7	2	111.67	5.73	-7.41	Low	1*	0.55
9j	609.07	12	7	2	111.67	5.98	-7.70	Low	1*	0.55
9k	613.03	12	8	2	111.67	5.99	-7.56	Low	1*	0.55
Zorifertinib	459.90	6	7	1	79.82	3.65	-5.50	High	0	0.55

RB – Rotable bonds; HAcc – H-bond acceptors; HDon – H-bond donors; Lipinski - Violation Lipinski Rule of 5; * - MW>500, [a]Log*s*-the water solubility of the compound. [b]GI-gastrointestinal absorption. [c]BS-bioavailability score.

Toxicity profile of the designed compound

As shown in **Table IV**, all designed compounds (**9a-9k**) exhibited a predicted LD_{50} of 2,000 mg/kg and a toxicity class of 4, whereas Zorifertinib showed an LD_{50} of 1,150 mg/kg (class 4). The average similarity of the designed compounds ranged from 54.91% to 58.50%, slightly higher than that of Zorifertinib (50.88%), with prediction accuracies around 67%. These results indicate that the designed compounds possess toxicity profiles comparable to or slightly better than the reference drug.

Table IV. Predicted toxicity properties of target compounds.

Compound	Predicted LD_{50} (mg/kg)	Predicted toxicity class (1 to 6)	Average similarity (%)	Prediction accuracy (%)
9a	2000	4	56.76	67.38
9b	2000	4	56.76	67.38
9c	2000	4	55.25	67.38
9d	2000	4	56.76	67.38
9e	2000	4	55.25	67.38
9f	2000	4	58.50	67.38
9g	2000	4	55.78	67.38
9h	2000	4	58.50	67.38
9i	2000	4	56.40	67.38
9j	2000	4	58.26	67.38
9k	2000	4	54.91	67.38
Zorifertinib	1150	4	50.88	67.38

CONCLUSIONS

Collectively, this study developed novel antitumor agents by designing and synthesizing a series of quinazoline-chalcone hybrids. Their antiproliferative

activity was evaluated against A549 and H1975 cell lines, with zorifertinib as the positive control. Molecular docking revealed their stable binding to EGFR, and ADME/Toxicity predictions validated their favorable drug-like and safety profiles, particularly for compound **9h**. However, the cytotoxicity was assessed only on cancer cell lines, and the selectivity against normal cells remains to be determined. Future work will address this limitation to establish their therapeutic selectivity index.

SUPPLEMENTARY MATERIAL

Additional data are available electronically at the pages of journal website: https://www.shd-pub.org.rs/index.php/JSCS/article/view/13582, or from the corresponding author on request.

Acknowledgements: This work was financially supported by the Natural Science Foundation of Liaoning Province (no. 20180550016), and the Scientific Research Foundation of the Education Department of Liaoning Province (no. LJGD2020015).

И З В О Д

ДИЗАЈН НОВИХ ХИБРИДА ХИНАЗОЛИНА И ХАЛКОНА КАО СНАЖНИХ ИНХИБИТОРА РЕЦЕПТОРА ЕПИДЕРМАЛНОГ ФАКТОРА РАСТА

YINGNUO WANG[1], JURANG LI[1], CHUNMENG LI[1], YANG LIU[1], ZHIQIANG CAI[1*], И SHUAI LI[2**]

[1]Liaoning Province Professional and Technical Innovation Center for Fine Chemical Engineering of Aromatics Downstream, School of Petrochemical Engineering, Shenyang University of Technology, Liaoning, Liaoyang 111003, P. R. China, и [2]Shandong Engineering Research Center of Pharmaceutical Green Intelligent Technology, Shandong Academy of Pharmaceutical Sciences, Shandong, Jinan 250101, P. R. China.

У оквиру овог истраживања успешно је дизајнирана и синтетисана нова серија хибрида хиназолина и халкона. Најважнија иновација је молекулска хибридизација фармакофорног скелета хиназолина са халконским фрагментом, чиме су створене нове хемијске врсте за испитивање потенцијалног синергистичког антитуморног ефекта. Успешно је спроведена усмерена синтеза у више реакционих корака. Први резултати испитивања показали су да већина синтетисаних хибрида показује снажну антипролиферативну активност *in vitro* према ћелијским линијама неситноћелијског рака плућа (NSCLC) (A549 и H1975). На основу испитивања молкулским докингом предложено је да је инхибиција рецептора епидермалног фактора раста (EGFR) главни механизам деловања и да једињења остварују стабилне интеракције са киназним доменом. Осим тога, *in silico* предвиђање апсорпције, дистрибуције, метаболизма и излучивања (ADME) и предвиђања токсичности добијена на SwissADME и ProTox 3.0 платформама редом, указују на то да једињења поседују особине сличне лековима и одговарајући профил безбедности. Ипак, цитотоксичност је одређена само према ћелијским линијама рака и селективност према нетуморским, здравим, ћелијама тек треба одредити. Без обзира на ова ограничења, почетни резултати су охрабрујући и упућују на наставак оптимизације и развој ових нових хибридних једињења.

(Примљено 13. октобра 2025; ревидирано 4. јуна 2026; прихваћено 13. августа 2026.)

REFERENCES

1. E. K. Chung, S. H. Yong, E. H. Lee, E. Y. Kim, Y. S. Chang, S. H. Lee, *Tuberc. Respir. Dis.* **86** (2023) 1 (https://doi.org/10.4046/trd.2022.0066)
2. K. Li, X. N. Cao, B. Ai, H. Xiao, Q. F. Huang, Z. Zhang, Q. Chu, L. Zhang, X. F. Dai, Y. D. Liao, *Thorac. Cancer* **12** (2021) 2161 (https://doi.org/10.1111/1759-7714.14044)
3. X. X. He, H. P. Ren, Y. Li, J. S. Lin, *CJin. J. Hepatolo.* **19** (2011) 561 (https://doi.org/10.3760/cma.j.issn.1007-3418.2011.08.001)
4. J. Z. Lin, L. C. Wu, X. Bai, Y. Xie, A. Q. Wang, H. H. Zhan1, X. B. Yang, X. H. Wan, X. Lu, X. T. Sang, H. T. Zhao, *Oncotarget* **7** (2016) 71036 (https://doi.org/10.18632/oncotarget.11954)
5. J. Zou, Y. Zeng, F. Wu, *Curr. Opin. Oncol.* **35** (2023) 22 (http://doi.org/10.1097/CCO.0000000000000914)
6. D. Das, J. Hong, *Eur. J. Med. Chem.* **170** (2019) 55 (https://doi.org/10.1016/j.ejmech.2019.03.004)
7. S. Wang, Y. Zhang, T. S. Ren, Q. Wu, H. Y. Lu, X. C. Qin, Y. Liu, H. Ding, Q. C. Zhao, *Cell Death Dis.* **16** (2025) 216 (https://doi.org/10.1038/s41419-025-07539-7)
8. G. Liu, S. Yang, B. Song, W. Xue, D. Y. Hu, L. H. Jin, P. Lu, *Molecules* **11** (2006) 272 (https://doi.org/10.3390/11040272)
9. L. L. Chi, Z. Q. Cai, B. Wang, W. T. Qin, Y. N. Wang, Q. Q. Feng, W. J. Ren, *J. Chem. Soc. Pak.* **45** (2023) 474 (https://doi.org/10.52568/001391/JCSP/45.06.2023)
10. M. W. Attwa, N. S. Al-Shakliah, H. AlRabiah, A. A. Kadi, A. S. Abdelhameed, *J. Pharm. Biomed. Anal.* **211** (2022) 114626 (https://doi.org/10.1016/j.jpba.2022.114626)
11. H. Ghouila, N. Meksi, W. Haddar, M. F. Mhenni, H. B. Jannet, *Ind. Crops Prod.* **35** (2012) 31 (https://doi.org/10.1016/j.indcrop.2011.05.026)
12. C. L. Zhuang, W. Zhang, C. Q. Sheng, W. N. Zhang, C. G. Xing, Z. Y. Miao, *Chem. Rev.* **117** (2017) 7762 (https://doi.org/10.1021/acs.chemrev.7b00020)
13. C. K. Wenzel, C. von Montfort, L. Ebbert, N. P. Klahm, A. S. Reichert, W. Stahl, P. Brenneisen, *Toxicol. In Vitro* **91** (2023) 105625 (https://doi.org/10.1016/j.tiv.2023.105625)
14. J. D. Zhai, B. X. Sun, F. Sang, *Front. Chem.* **10** (2022) 964089 (https://doi.org/10.3389/fchem.2022.964089)
15. E. B. Mass, G. V. Duarte, D. Russowsky, *Mini Rev. Med. Chem.* **21** (2021) 186 (https://doi.org/10.2174/1389557520666200730160325)
16. A. Thiriveedhi, R. V. Nadh, N. Srinivasu, K. Kaushal, *Lett. Drug Des. Discovery* **15** (2018) 757 (https://doi.org/10.2174/1570180814666171013162148)
17. S. Madhavi, R. Sreenivasulu, R. R. Raju, J. P. Yazala, *Saudi Pharm. J.* **25** (2017) 275 (https://doi.org/10.1016/j.jsps.2016.06.005)
18. R. Thomas, W. H. Zhang, *Front. Oncol.* **9** (2019) 800 (https://doi.org/10.3389/fonc.2019.00800)
19. A. M. Wasserman, J. Bajorath, *Future Med. Chem.* **3** (2011) 425 (https://doi.org/10.4155/fmc.10.293)
20. A. M. Wassermann, J. Bajorath, *Med. Chem. Comm.* **2** (2011) 601 (https://doi.org/10.1039/c1md00066g)
21. J. Althaus, T. Hake, M. Lehr, *J. Enzyme Inhib. Med. Chem.* **31** (2016) 131 (https://doi.org/10.1080/14756366.2016.1178246)

22. A. Detsi, V. Roussis, A. Tsotinisc, C. Roussakis, T. Calgeropoulou, *Synlett* **20** (2005) 3131 (https://doi.org/10.1055/s-2005-921933)
23. K. Lu, Y. T. Ma, M. L. Gao, Y. Liu, C. M. Xu, X. Zhao, P. Yu, *Org. Lett.* **18** (2016) 5038 (https://doi.org/10.1021/acs.orglett.6b02493)
24. A. Mozo-Villarías, J. Cedano, E. Querol, *Eur. Biophys. J.* **50** (2021) 951 (https://doi.org/10.1007/s00249-021-01557-x)
25. L. Xie, D. L. Yang, Q. Y. Lu, H. B. Zeng, *Curr. Opin. Colloid Interface Sci.* **47** (2020) 58 (https://doi.org/10.1016/j.cocis.2019.12.001)
26. Q. Sun, Y. F. Fu, W. Q. Wang, *Chem. Phys.* **559** (2022) 111550 (https://doi.org/10.1016/j.chemphys.2022.111550)
27. R. L. Yang, J. J. Ma, H. Guo, Q. H. Meng, Y. W. Wang, H. Yan, R. Y. Jin, Z. Li, L. J. Meng, *Nat. Prod. Commun.* **17** (2022) 1934578X211059645 (https://doi.org/10.1177/1934578X211059645)
28. A. Dang, S. Dang, B. N. Vallish, *Rev. Recent Clin. Trials* **16** (2021) 193 (https://doi.org/10.2174/1574887115999201103200248)
29. J. Cui, Y. F. Hu, Y. H. Guo, J. W. Ma, K. J. Nan, H. Y. Zhang, *Tumor Biol.* **35** (2014) 11701 (https://doi.org/10.1007/s13277-014-2660-z)
30. B. Zhang, Z. Liu, S. Xia, Q. Liu, S. Gou, *Eur. J. Med. Chem.* **216** (2021) 113300. (https://doi.org/10.1016/j.ejmech.2021.113300)
31. A. H. Abou-Zied, B. G. Youssif, F. M. Mohamed, A. M. Hayallah, M. Abdel-Aziz, *Bioorg. Chem.* **89** (2019) 102997 (https://doi.org/10.1016/j.bioorg.2019.102997)
32. Y. Li, Y. Sun, Y. Zhou, X. Li, H. Zhang, G. Zhang, *J. Enzyme Inhib. Med. Chem.* **36** (2020) 207 (https://doi.org/10.1080/14756366.2020.1852556)
33. T. Ishida, *Chem. Biodivers.* **2** (2005) 569 (https://doi.org/10.1002/cbdv.200590038)
34. X. Wang, Y. Zheng, X. Xu, S. Gao, J. Wang, Q. Gou, *J. Mol. Struct.* **1254** (2022) 132322 (https://doi.org/10.1016/j.molstruc.2021.132322)
35. M. Abdel-Aziz, S. E. Park, G. E. D. A. A. Abuo-Rahma, M.H. Sayed, Y. Kwon, *Eur. J. Med. Chem.* **69** (2013) 427 (https://doi.org/10.1016/j.ejmech.2013.08.040).